International Journal of Nanomedicine

Dovepress
Taylor & Francis Group

Open Access Full Text Article

ORIGINAL RESEARCH

Enhanced Bioavailability of a Thionated IMiD Derivative Nanosuspension for Parkinson's Disease Targeting α-Synuclein

Luca Casula[1], Maria Francesca Palmas[2], Maria Cristina Cardia[1], Donatella Valenti[1], Elena Pini[3], Michela Etzi[2], Salvatore Marceddu[4], Chiara Sinico[1], David Tweedie[5], Nigel H Greig[5], Dong Seok Kim[6,7], Anna Rosa Carta[2], Francesco Lai[1]

[1]Department of Life and Environmental Sciences, University of Cagliari, Cagliari, Italy; [2]Department of Biomedical Sciences, University of Cagliari, Cagliari, Italy; [3]Departmentof Pharmaceutical Sciences, University of Milan, Milan, Italy; [4]Institute of Sciences of Food Production (ISPA-CNR), Baldinca (Sassari), Italy; [5]Drug Design & Development Section, Translational Gerontology Branch, Intramural Research Program, National Institute on Aging, National Institutes of Health, Baltimore, MD, USA; [6]AevisBio, Inc., Gaithersburg, MD, USA; [7]Aevis Bio, Inc., Daejeon, Korea

Correspondence: Francesco Lai, Department of Life and Environmental Sciences, University of Cagliari, S.P. Monserrato-Sestu km 0.700, Cagliari, 09042, Italy, Email frlai@unica.it

Introduction: Chronic neuroinflammation and the accumulation of misfolded α-synuclein are hallmarks of Parkinson's disease (PD), a progressive neurodegenerative disorder that leads to neuronal loss and dysfunction. Immunomodulatory imide drugs (IMiDs) are thalidomide analogs that exhibit potent anti-inflammatory and neuroprotective effects by regulating NF-κB and TNF-α levels. However, their therapeutic use is limited by their teratogenic actions mediated via Cereblon (CRBN) binding. Previous studies have demonstrated the efficacy of pomalidomide (POM) in mitigating neuroinflammation and providing neuroprotection in a rodent model of PD. Building on these findings, a novel derivative, 3-monothiopomalidomide (MTPOM), was synthesized, with reduced teratogenic potential compared to POM. Nevertheless, like other IMiDs, MTPOM shows poor aqueous solubility and low gastrointestinal bioavailability following oral administration.

Methods: MT-POM was formulated as a nanosuspension (NS) via wet ball media milling using Tween 80 as a stabilizer. The morphology of nanocrystals was characterized by SEM, while the average diameter, size distribution and zeta potential were assessed via DLS and M3-PALS. The crystalline/amorphous nature was investigated by means of ATR-FT-IR and XRPD. Moreover, the aqueous solubility and dissolution rate were tested in vitro, and plasma and brain concentrations were evaluated in rats.

Results: The produced NS (~226 nm, PDI 0.22, zeta potential −26 mV) demonstrated enhanced aqueous solubility and dissolution rate compared to the raw drug. MTPOM retained crystallinity and showed optimal stability over 60 days of storage. Pharmacokinetic studies in rats established that MTPOM-NS provided significantly higher plasma and brain concentrations, prolonged systemic exposure, and greater drug accumulation in brain tissue.

Conclusion: This enhancement in bioavailability supports the formulation of NS as a promising strategy for CNS-targeted therapies, providing a strong rationale for further investigation into the efficacy of MTPOM-NS in the chronic treatment of PD, which will be the focus of future studies.

Keywords: 3-Monothiopomalidomide, nanocrystals, Parkinson's disease, brain delivery, immunomodulatory imide drugs, IMiDs, pomalidomide

Introduction

Parkinson's disease (PD) is classified among synucleinopathies, a subgroup of neurodegenerative disorders characterized by the abnormal accumulation and aggregation of misfolded α-synuclein (α-syn) protein within neurons and other brain cells. This pathological α-syn deposition disrupts cellular function and is a central contributor to disease pathology. A hallmark feature of neurodegenerative synucleinopathies is chronic neuroinflammation, which contributes to neuronal loss and dysfunction. This neuroinflammatory process is considered to drive disease progression[1,2] and impact key functions such as

Received: 29 May 2025
Accepted: 13 October 2025
Published: 20 November 2025

Graphical Abstract

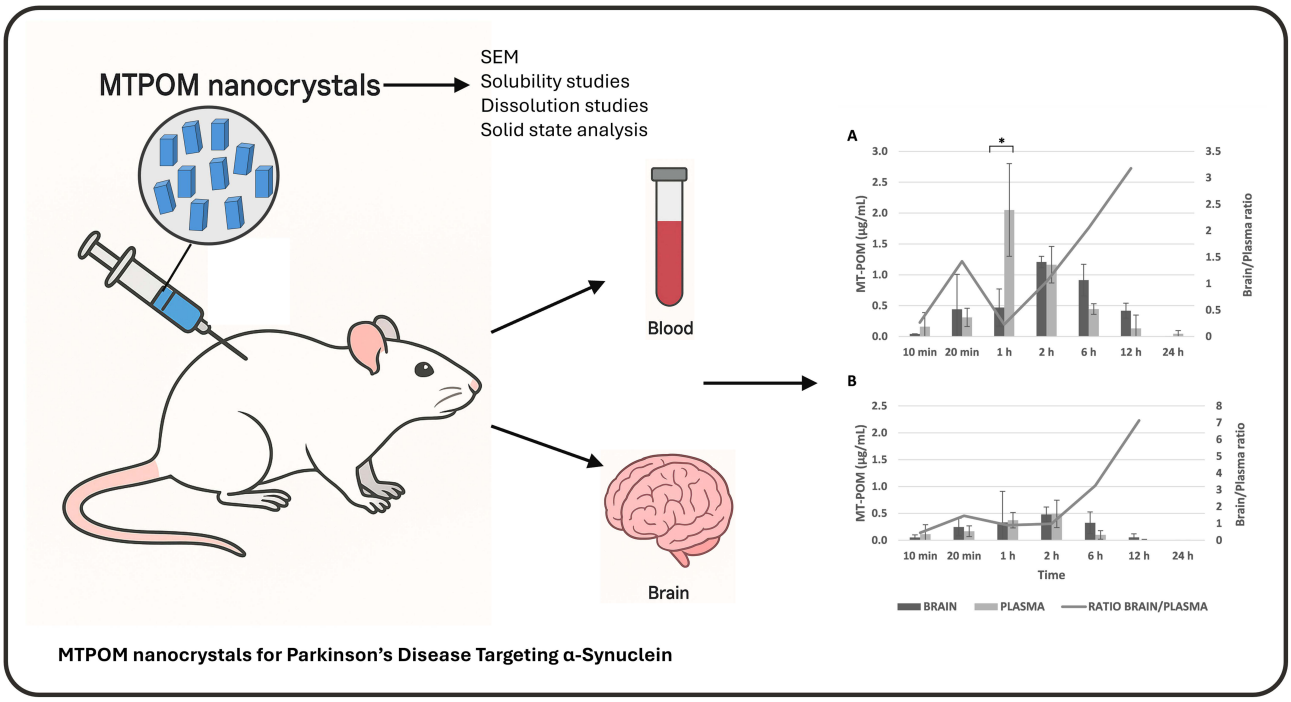

motor coordination, memory, and cognition.[3] Recent findings suggest that α-syn can impact neuroinflammation and neurodegeneration, through the recruitment and activation of CNS resident immune cells, namely microglia. This pathological cross-talk between reactive glial cells and neurons occurs through the release of pro-inflammatory signaling molecules, including the cytokines TNF-α, interleukin (IL)-1β, and IL-6.[4,5]

Therefore, agents that can regulate the production and release of proinflammatory cytokines, or cytokine-blocking molecules, are considered as promising neuroprotective strategies.[6–10] Among these, immunomodulatory imide drugs (IMiDs) have garnered significant attention. These thalidomide-based analogs, including pomalidomide (POM) and lenalidomide, exhibit a range of pharmacological properties beneficial in the treatment of multiple myeloma, including potent anti-proliferative, anti-angiogenic, immune-modulating, and notably, anti-inflammatory effects.[11,12] Recently, POM has been reported to mitigate neuroinflammation and providing neuroprotection in preclinical models of neurodegenerative and neuroinflammatory disorders.[13–16] The pharmacological actions of IMiDs are partly mediated by the downregulation of the transcription factor NF-κB and an increased degradation of TNF-α mRNA, resulting in reduced TNF-α protein levels and, in turn, attenuation of the inflammatory cascade.[12,17] Moreover, numerous actions of IMiDs are mediated via their binding to Cereblon (CRBN), the substrate recognition element of the E3 cullin 4-RING ubiquitin ligase complex.[18–21] IMiDs binding to human CRBN triggers the ubiquitination and ensuing proteasomal degradation of key neosubstrates, largely zinc finger transcription factors, that underpin the anticancer activity of thalidomide-like agents, but also underlie their teratogenic effects.[18–21]

A newly synthesized thalidomide derivative based on the backbone of POM, the most potent clinically available anti-inflammatory IMiD, is 3-monothiopomalidomide (MTPOM).[22] With respect to POM, MTPOM retains potent anti-inflammatory activity. However, unlike the parent compound, MTPOM binds to human CRBN without triggering the subsequent degradation of key neosubstrates such as SALL4 and Aiolos, which are well-established mediators of IMiD-CRBN-dependent teratogenic and anticancer effects.[23] This selective CRBN engagement confers a significantly attenuated risk of teratogenicity, as recently demonstrated in embryonic models.[22] Thus, MTPOM presents an improved toxicological profile while preserving immunomodulatory efficacy sufficient for therapeutic applications. These properties make MTPOM a strong candidate for targeting disorders characterized by robust systemic and neuroinflammatory pathology, while

addressing critical safety limitations of current POM formulations and advancing the development of safer immunomodulatory therapies.

Like other IMiDs, POM and MTPOM are characterized by a poor aqueous solubility, resulting in reduced gastrointestinal absorption after oral administration,[24,25] and a reduced ability to be administered by other routes. Indeed, poor water solubility represents a major challenge in drug development and clinical translation, prompting extensive efforts to develop suitable delivery systems or nanocarriers including liposomes, cyclodextrins, cubosomes, and polymeric nanoparticles.[26–30] In particular, nanoparticles have shown considerable promise in overcoming the blood-brain barrier (BBB), a highly selective system that tightly regulates the passage of ions, small molecules, and macromolecules from the blood to the brain. While the BBB restricts the delivery of most conventional drugs, nanoparticles can facilitate enhanced brain penetration, making them especially attractive for the treatment of neurological disorders.[31,32] An alternative and successful approach is the production of pure drug nanoparticles devoid of matrix materials, formerly referred to as drug nanocrystals.[33,34] Nanocrystals are characterized by an average diameter below 1 μm (typically in the range of 200–500 nm)[35–37] and are typically prepared as an aqueous nanosuspension (NS) using either top-down or bottom-up techniques, with polymers or surfactants to stabilize them.[38–41]

In our previous study[42] we successfully developed a POM-NS via wet ball media milling, producing homogeneously dispersed nanocrystals (219 nm, polydispersity index [PDI] 0.21), with enhanced solubility and dissolution rate compared to the raw drug. This formulation achieved higher plasma and brain concentrations following intraperitoneal administration in rats. Its efficacy as a chronic treatment was then tested in a neuropathological rodent model of PD,[43] providing compelling evidence of POM's disease-modifying potential, including improved motor performance, reduced nigrostriatal degeneration and mitigation of inflammation. Despite its therapeutic benefits, POM, like most IMiDs is associated with serious side effects like teratogenicity,[44–46] highlighting the urgent need for next-generation IMiD-based therapies with improved safety profiles.

The aim of the current study was to improve the aqueous solubility and bioavailability of MTPOM by developing a NS for optimal peripheral administration and enhanced CNS bioavailability. The resulting formulation was fully characterized for nanocrystals morphology, average diameter, size distribution and zeta potential. Additionally, the crystalline/amorphous nature of the drug, its saturation solubility and dissolution rate were evaluated. Finally, in vivo studies were performed in adult male Sprague-Dawley rats to assess plasma and brain concentrations following intraperitoneal administration.

Materials and Methods

Materials

Polysorbate 80 (Tween 80) was purchased from Galeno (Comeana, Italy). Acetonitrile, DMSO, and all the other products were supplied by Sigma Aldrich (Milan, Italy). MTPOM was provided by Aevis Bio Inc. (Republic of Korea).[22]

Methods

Preparation and Characterization of MTPOM-NS

The wet media milling technique was used to obtain the MTPOM nanosuspension (MTPOM-NS).[39,47] Firstly, 5 mL of a coarse suspension was obtained by dispersing the bulk drug 1% (w/w) in an aqueous Tween 80 solution (0.5% w/w) under vortex mixing for 12 minutes. The suspension was then aliquoted into Eppendorf microtubes, each containing 1 mL of the obtained coarse suspension (equivalent to 10 mg of drug) and 0.5 g of yttrium-stabilized zirconia-silica beads (Silibeads® Type ZY Sigmund Lindner, Germany) with a diameter of 0.1–0.2 mm. A beads-milling cell disruptor (Disruptor Genie®, Scientific Industries, USA) was used to oscillate the microtubes for 60 minutes at 3000 rpm. The resulting NS was then separated from the zirconia-silica beads by sieving. Particle size (mean diameter) and PDI, reflecting the width of the size distribution, were then measured by dynamic light scattering (DLS) using a Zetasizer nano (Malvern Instruments, Worcestershire, UK). Zeta potential was also determined with the same instrument using the M3-PALS (Phase Analysis Light Scattering) method. MTPOM-NS was diluted with bi-distilled water (1:100) immediately

before analysis. The suspension was stored at 4° C and underwent a 60-day stability study wherein mean diameter, PDI, Zeta potential and drug concentration were monitored.

Scanning Electron Microscopy

Scanning electron microscopy (SEM) was used to assess the morphology of bulk MTPOM and the corresponding nanocrystals.[33,48] Using carbon adhesive discs, bulk MTPOM was deposited on an aluminum stub and then coated with gold using an Agar Automatic Sputter Coater B7341. The sample was analyzed using an environmental scanning electron microscope (Zeiss EVO LS 10, Oberkochen, Germany) running at 20 Kv in high vacuum mode with a secondary electron detector [SEI]. To assess the nanocrystals morphology, a drop of MTPOM-NS was placed on a slide, allowed to air dry, and then coated with gold using the previously mentioned sputter coater. The sample was, thereafter, examined using the same protocol.

Solubility Studies

The aqueous solubility of MTPOM in its raw powder form, as well as in coarse and NS formulations, was evaluated.[35,42] An excess amount of MTPOM raw powder was dispersed in 1.2 mL of bidistilled water. This raw suspension, along with the MTPOM coarse suspension and NS, was kept under constant stirring at 37 °C for 72 hours. After incubation, 1 mL of each sample was collected and centrifuged at 15,000 rpm for 30 minutes. The resulting supernatant was transferred to fresh microtubes and subjected to a second centrifugation under the same conditions. A known volume of the final clear supernatant was then appropriately diluted and analyzed by HPLC to quantify MTPOM content (n = 3).

Dissolution Studies

The dissolution rate of MTPOM (as NS, coarse suspension and raw powder) was evaluated in phosphate buffer solution (PBS, pH of 7.4) according to previous published protocols with minor modifications.[41,49,50] To ensure equivalence between the amount of raw powder and the tested volume of the liquid formulations, the latter were analysed via HPLC to confirm that the concentration was consistent with the expected theoretical one.

Once confirmed, 100 µL of MTPOM-NS, MTPOM coarse suspension, and 1 mg of MTPOM (corresponding to 100 µL of NS or coarse suspension) were added to 100 mL of PBS in thermostated release cells. The amount of MTPOM and release medium were calculated in order to maintain sink conditions. Throughout the investigation, the release cells were maintained at 37 °C and continuously stirred with a magnetic stirrer. At predetermined time points (1, 5, 10, 20, 30 minutes, and 1, 2, 4, 6, 8 hours) 2 mL samples were withdrawn and immediately centrifuged at 15000rpm for 20 minutes to separate the undissolved drug. To maintain sink conditions, an equal volume of fresh medium was added after each withdrawal. The supernatant of the centrifuged withdrawn samples was then analyzed using the HPLC method described below.

Drug Quantification in the in vitro Samples

MTPOM content for all the in vitro experiments (drug quantification in the formulations, stability tests, solubility and dissolution tests) was evaluated using an Alliance 2690 chromatograph (Waters, Italy) equipped with a photodiode array detector and a computer integrating software (Empower 3). Using a Sunfire C18 column (3.5 µm, 4.6 mm × 150 mm, Waters), and a mobile phase of water: ACN: Acetic acid =20: 84.5: 0.5, eluted at a flow rate of 0.7 mL/min, MTPOM was determined at 306 nm wavelength. Standard solutions were used to generate a standard calibration curve, which was plotted using linear regression analysis, producing a correlation coefficient value (R^2) of 0.999.

Solid State Analysis

The MTPOM-NS was frozen at −30 ◦C and freeze-dried using a Lyovapor L200 (Buchi, Milan, Italy) to obtain a solid powder for the solid-state analysis. Using a Perkin Elmer Spectrum One FT-IR (Perkin Elmer, Waltham, MA, USA) equipped with a Perkin Elmer Universal ATR sampling accessory made of a diamond crystal, ATR-FT-IR spectra were obtained by placing the sample directly on the surface of the diamond without further preparation. Analyses were conducted using the transmittance technique with 32 scansions and a 4 cm^{-1} resolution, covering a spectral region between 4000 and 650 cm^{-1}.

XRPD analyses were conducted using a Rigaku MiniFlex diffractometer with a CuKα radiation detector (λ = 1.54056 Å) as the X-ray source, operating with a 30 kV voltage and a 15 mA current, respectively. The solid samples to be submitted to the XRPD analysis were gently grinded in a mortar, transferred into the sample holder and the powder pressed into to create a uniform and flat surface. In the range of 3 to 60 °C 2θ (deg), measurements were made at a scan angular speed in steps of 0.02, using a scan step time of 2.00 s. The diffractograms show the peak intensity as a function of 2θ.EC.

Pharmacokinetic Studies

Male Sprague-Dawley rats (275–300 g) were housed in groups of four, acclimated to 21 ± 1 ◦C and maintained on a 12-hour light/dark cycle, with lights on at 7:00 a.m and with water and food available ad libitum. All experimental procedures followed the protocols and guidelines approved by the European Community (2010/63UE L 276 20/10/2010) and complied with the ARRIVE guidelines. The Ministry of Health authorized the experimental protocols under Authorization No. 766/2020-PR (D. Lgs. 26/2014).

Animals were randomly divided into groups of three to receive a single intraperitoneal injection of either MTPOM-NS (5 mg/kg) or the corresponding coarse suspension (MTPOM-CS, 5 mg/kg) at a concentration of 10mg/mL (injection volume for a ~300 g rat was approximately 0.15 mL). Following treatment, animals were deeply anesthetized and sacrificed by decapitation after 10, 20 minutes, 1, 6, 12, 24 and 48 hours, in order to collect blood and brain samples. Plasma was obtained by centrifugation (10,000g, 1 minute, 4°C) and, together with brain samples, immediately stored at −80 °C.[42]

Drug Quantification in Biological Samples

Biological blood and brain samples were processed for drug quantification using a previous protocol with minor modifications.[42]

Preparation of Blood Samples for HPLC Analyses

700 µL of heparinized plasma samples were treated with 500 µL of a 50% ACN/DMSO mixture and vortexed for two minutes. The mixture was centrifuged for 30 minutes at 15,000 rpm and 4°C and the resulting supernatant was transferred into HPLC vials for drug quantification.

Preparation of Brain Samples for HPLC Analyses

The brain of each rat was thawed, carefully weighed, and shredded in a mortar using a pestle. The tissue was then treated with 6 mL of 50% ACN/DMSO mixture and collected in a tube. Homogenization was performed by vortexing 30 minutes (6 cycles of 5 minutes each), using an ice bath, between cycles, to prevent overheating. The obtained samples were divided into five Eppendorf tubes and centrifuged for 30 minutes at 15,000 rpm (4°C). The supernatant was collected and transferred to test tubes for HPLC analysis.

HPLC Analyses

A PerkinElmer HPLC Series 200, equipped with a UV-VIS detector and a computerized data integration system (TotalChrom Navigator), was used to quantify MTPOM biological samples. The mobile phase and workflow were the same as previously described in paragraph 2.4, whereas the column was an InertClone 5 µm ODS (2) 150 Å LC Column 150×4.6 mm (Phenomenex). MTPOM was revealed at a wavelength of 306 nm and the standard calibration curve was created using the working standard solutions. The obtained calibration graphs were plotted using linear regression analysis, yielding a correlation coefficient (R2) value of 0.999.

Pharmacokinetic Analysis

After a single intraperitoneal (i.p.) administration of MTPOM-NS or MTPOM-CS, pharmacokinetic parameters (PK) were calculated using the PK-Solver software (in the non-compartmental analysis mode) and the MTPOM mean plasma concentration (n = 3 determinations at each time point). The $AUC_{0-\infty}$ (the total area under the drug plasma concentration–time curve) was determined using the trapezoidal method, and the elimination half-life ($T_{1/2}$) was calculated as 0.693/elimination rate constant.[51]

Statistical Analysis of Data

For the stability, solubility and dissolution studies, each experiment was performed at least in triplicate, and the results are shown as means ± SD. Student's *t*-test was utilized to compare two samples, while one-way ANOVA followed by Tukey's HSD post-hoc test was applied for multiple comparisons. Data were analyzed using XL Statistic for Microsoft Excel. A statistical significance level of 0.05 was chosen. The similarity factor (f_2), a statistically derived mathematical parameter, was used to compare the dissolution profiles of the different samples:[52]

$$f_2 = 50 \times \log\left\{\left[1 + \frac{1}{n}\sum_{t=1}^{n}(S_{1t} - S_{2t})^2\right]^{-0.5} \times 100)\right\}$$

where n is the number of time points, S_{1t} is the released percentage of the drug in sample 1, and S_{2t} is the released percentage of the drug in sample 2, at time t. The same time-points were used for the evaluation of the dissolution profiles, which were completed at the first sampling time when drug dissolution was ≥85%. According to the European Medicines Agency and the US Food and Drug Administration, f_2 value between 50 and 100 indicated that the two curves are identical or equivalent.[53,54]

Results and Discussion

Preparation and Characterization of MTPOM-NS

A wet ball media milling technique was used in this work to produce MTPOM-NS using the non-ionic surfactant Tween 80. The drug-to-stabilizer ratio was 2:1, corresponding to concentrations of 1% and 0.5% (w/w), respectively (Table 1). The DLS analysis of the obtained NS revealed the presence of nanocrystals with an average diameter of 226 nm and a PDI of 0.22, indicating a relatively narrow size distribution. Since the zeta potential revealed a promising stability of the colloidal system, the formulation was monitored over a period of 60 days to evaluate any possible changes in the average diameter, PDI and zeta potential. As shown in Figure 1, no significant changes in the dimensional properties of the formulation were observed. Moreover, MTPOM-NS zeta potential maintained a negative value (−26/-29 mV) throughout the 60-day storage period. HPLC analysis further confirmed the stability of the formulation, showing no changes in the concentration, retention time or the absence of additional peaks, suggesting no decomposition or formation of degradation products.

To evaluate morphological changes in MTPOM crystals after milling, the bulk drug and the resulting NS were inspected via SEM (Figure 2). MTPOM bulk powder appeared as irregular, elongated fibrillar crystals with variable dimensions greater than 10 μm. In contrast, the nanocrystals appeared as quasi-spherical particles, with homogeneous and regular surfaces, and diameter values consistent with those measured by dynamic light scattering. In a similar manner, posaconazole, a poorly soluble antifungal drug, exhibits an elongated needle-like crystals morphology, but is fractured into small homogeneous nanostructures when nanosized via media milling, with a resulting average diameter of 185 nm.[55]

Solid State Analysis

Solid state characterization of freeze dried MTPOM-NS, as well as its components in a raw form and in the physical mixture, was performed by ATR-FTIR, and XRPD to evaluate any possible interactions among the used substances, or modifications induced by NS production.

The overlapping IR spectra of the different samples are shown in Figure 3, while the individual spectra, provided for a more detailed peak analysis, are available in Supplementary Figures 1–4. As shown in Figure 3, the N-H_2 and N-H stretching

Table 1 Composition and Characterization of MTPOM-NS

	Composition % (w/w)		Characterization		
	MTPOM	TWEEN 80	Average Diameter (nm)	PI	Zeta Potential (mV)
MTPOM-NS	1	0.5	226 ± 18	0.220 ± 0.01	−26 ± 2

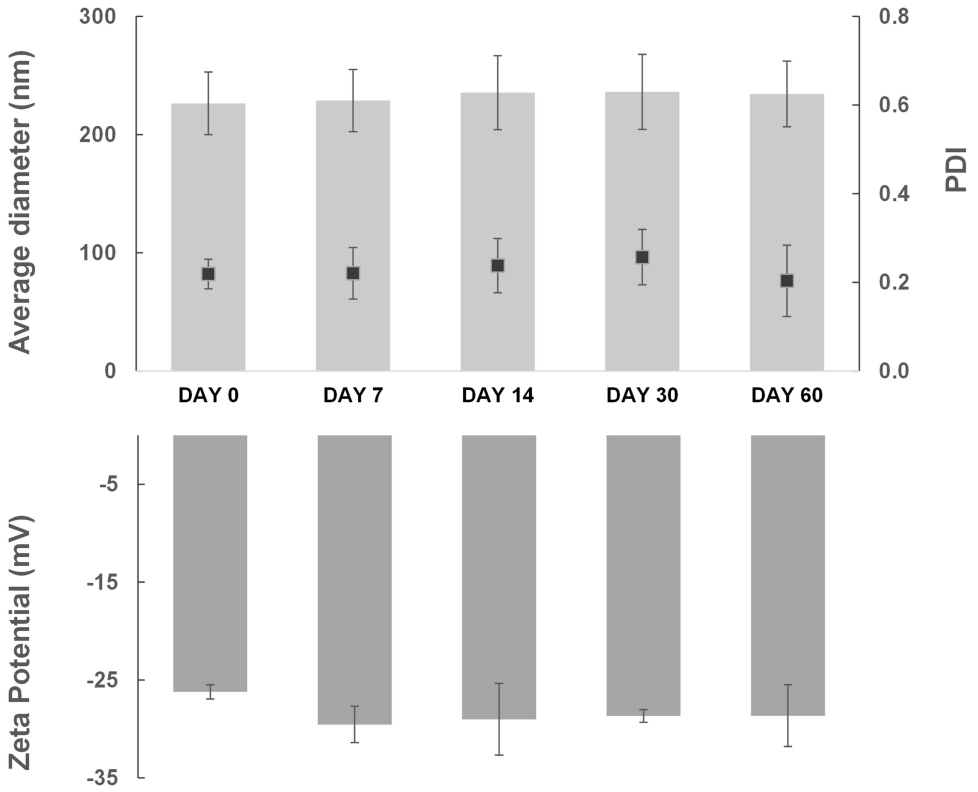

Figure 1 Stability of the MTPOM-NS in terms of average diameter (nm), PI and zeta potential (mV) over 60 days of storage at 4 °C.

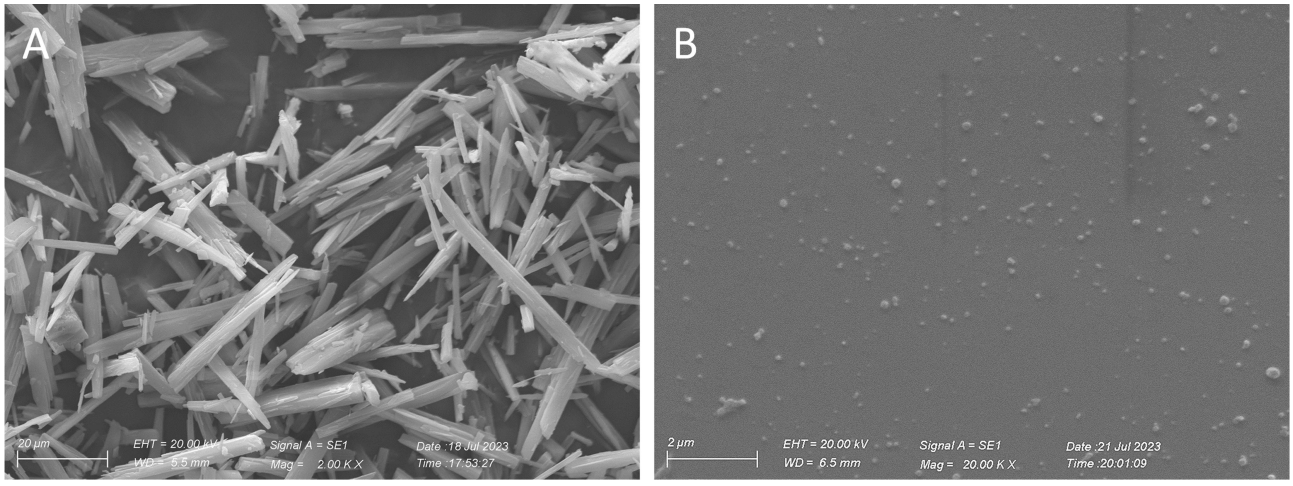

Figure 2 SEM images of MTPOM as (**A**) a bulk powder and (**B**) MTPOM-NS.

bands of MTPOM appear at 3432, 3396 and 3181 cm^{-1}, respectively; the aromatic CH stretching vibrations occur at 3082 cm^{-1}, while the aliphatic ones appear at 2901 and 2869 cm^{-1}. The C=O and the thioamide stretchings are detected at 1728, 1692 and 1480 cm^{-1}, respectively. The C-N stretching modes are assigned at 1354 cm^{-1}.

Regarding the Tween 80 (T80) spectrum, the broad O-H band can be found at 3493 cm^{-1}, the Csp^3-H stretchings at 2922 and 2857 cm^{-1}, whereas at 1735 and 1096 cm^{-1} the C=O and C-O bands are well distinguished, together with the C-H bending at 1456 and 1349 cm^{-1}.[56]

https://doi.org/10.2147/IJN.S543652

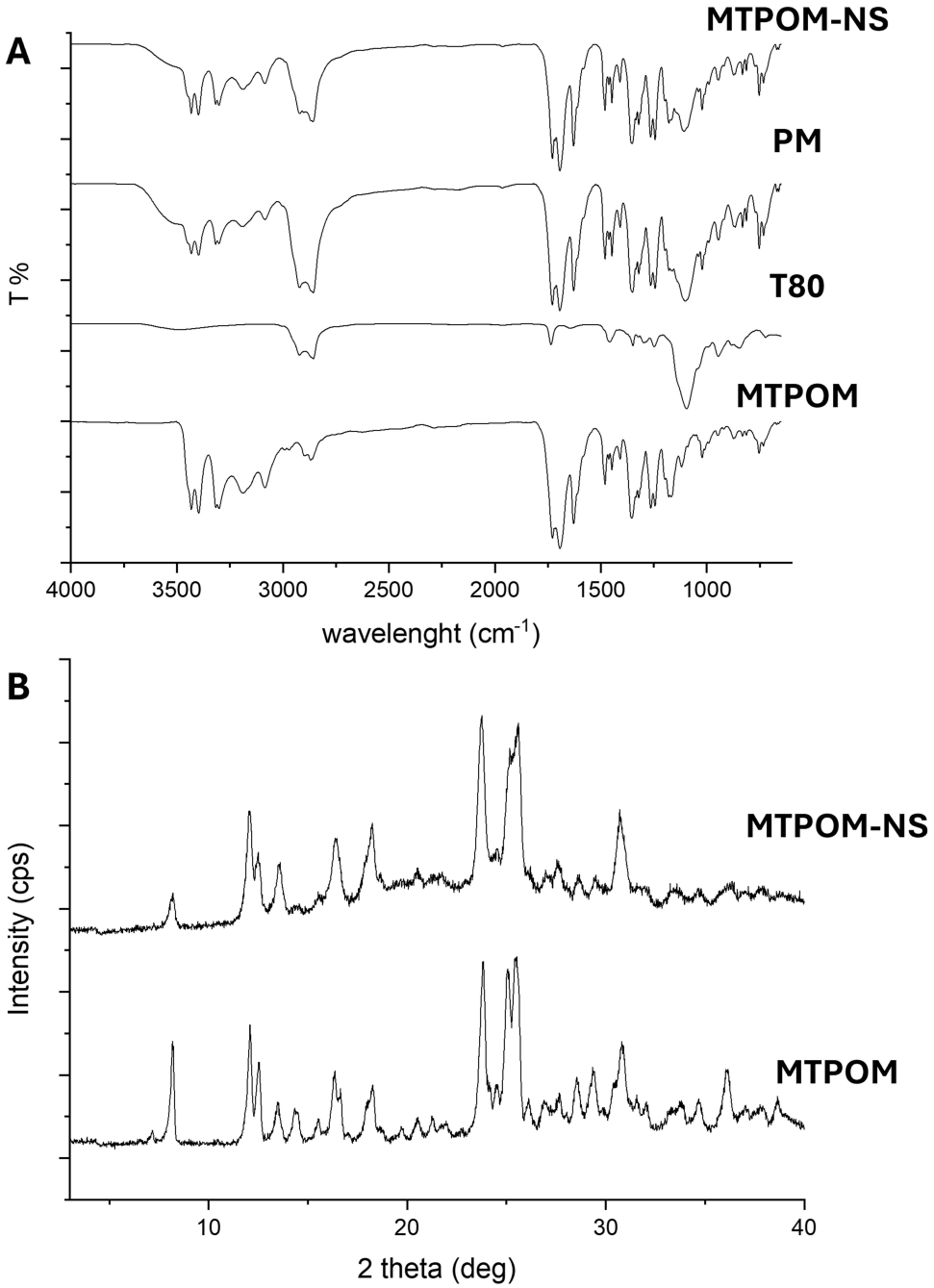

Figure 3 (**A**) FTIR, (**B**) XRPD analyses of MTPOM, tween 80 (T80), physical mixture (PM) and MTPOM-NS.

Since the FTIR spectra of the physical mixture and NS are essentially superimposed on those of the individual components, with no new peaks observed, it can be concluded that there no interactions occur between the drug and the excipient.

XRPD analyses of MTPOM confirm its crystalline profile, with reflection peaks at 8.12, 12.00, 13.52, 16.34, 25.56. The diffractograms of MTPOM-PM and MTPOM-NS indicate that POM retains its crystallinity in both preparations, indicating that the formulation process does not change its solid state.[57]

Solubility and Dissolution Studies

The reduction in crystals size − obtained through the high shear forces generated during the milling process − leads to an increase in the saturation solubility of hydrophobic drugs, which − as demonstrated by in vivo studies − results in enhanced bioavailability.[48] As illustrated in Figure 4, MTPOM showed a very low aqueous solubility of 4.8 ± 0.2 µg/mL as raw drug. This was slightly increased to 9.3 ± 0.3 µg/mL when MTPOM was formulated as a coarse suspension. By contrast, MTPOM-NS demonstrated a solubility value of 27.0 ± 1.3 µg/mL, which is 5.7-fold higher than the raw material. These findings indicate that the enhanced solubility is primarily due to nanosizing of the crystals, with the surfactant playing an additional, but secondary role, in accordance with the Freundlich-Ostwald equation.[37]

Once the increased saturation solubility of the obtained nanocrystals was verified, dissolution rate, a critical parameter for predicting drug bioavailability, was evaluated.[58] To closely mimic peritoneal conditions, the test was performed at 37 °C in PBS (pH of 7.4), with the sample-to-medium ratio carefully chose to maintain sink condition. This corresponds to a release medium volume at least 3–10 times greater than the saturation volume.[59] As for the solubility test, the raw drug and the coarse suspension were also evaluated to assess the impact of the stabilizer on the dissolution profile.

When used as the raw drug, MTPOM showed a modest dissolution, with approximately 22% released within the first minute of evaluation, and a gradual increase to 44% over 8 hours (Figure 5). Similarly, the coarse suspension exhibited a dissolution of 23% at the first time point, reaching 47% at the end of the test. To investigate the resemblance of the two curves, the similarity factor (f_2) was calculated and resulted in a value of 69, thereby confirming the similarity of the dissolution profiles of the two samples. On the other hand, a rapid dissolution of MTPOM nanocrystals (MTPOM-NS) was observed, with 82% of the drug dissolving after one minute, and values higher than 90% achieved after 4 hours of testing. Similarly, Liu et al observed almost complete dissolution of indomethacin and itraconazole after one minute of testing when formulated as nanosuspensions using Tween 80 as stabilizer. In contrast, the corresponding coarse suspensions showed a dissolution of approximately 20% after one minute, and 40–50% after 30 minutes.[60] In the current study, given the markedly increased solubility and rapid dissolution of MTPOM in its NS form, and considering that nanosizing can improve drug absorption,[61] the bioavailability of MTPOM-NS was hence evaluated following intraperitoneal administration.

In vivo Studies

Time-dependent in vivo data were obtained after a single intraperitoneal injection of MTPOM formulated as either a NS or a coarse suspension (MTPOM-NS or MTPOM-CS), in order to compare the systemic and brain bioavailability of the two formulations. In this regard, the intraperitoneal route was chosen in order to mimic oral administration, in terms of portal

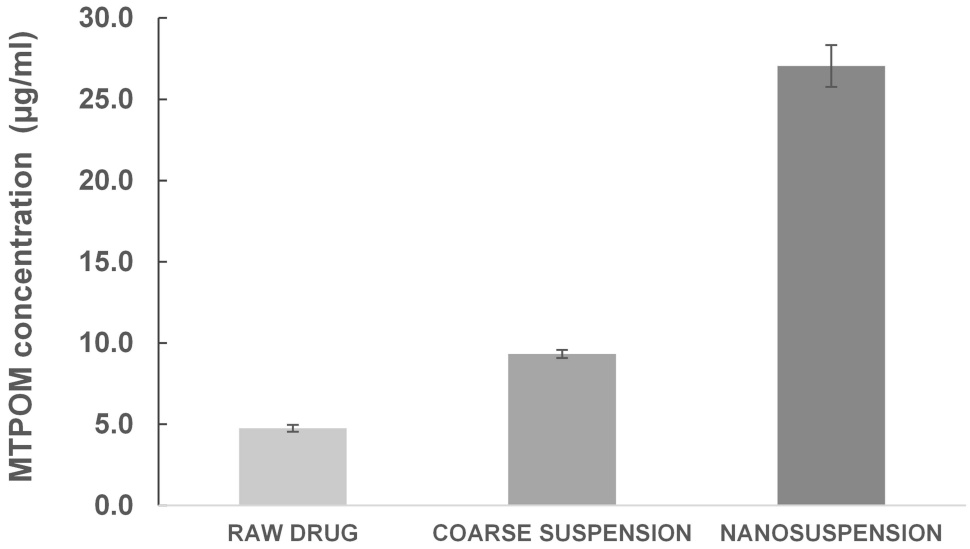

Figure 4 Solubility of MTPOM at 37 °C as raw drug, coarse suspension and MTPOM-NS.

https://doi.org/10.2147/IJN.S543652

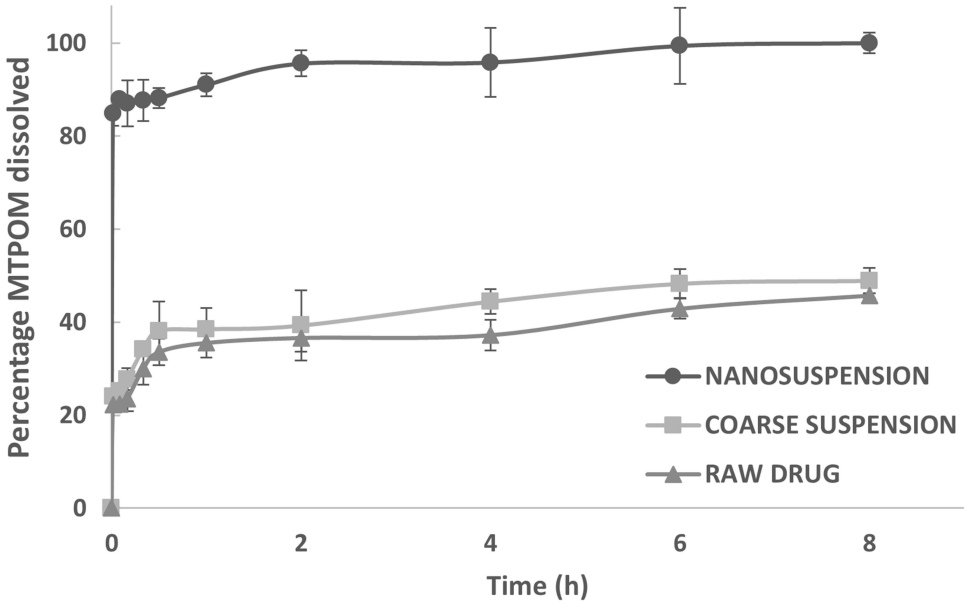

Figure 5 Dissolution profiles of raw MTPOM, MTPOM coarse suspension and MTPOM nanosuspension (MTPOM-NS).

adsorption and first-pass liver metabolism while ensuring a homogeneous interindividual bioavailability in comparison to oral intake.[62] Drug was extracted from time-dependent (10, 20 min, 1, 2, 6, 12, 24 and 48 h) biological samples, which was then analysed and quantified by HPLC. The obtained data were thereafter analysed using PK-Solver software to calculate the pharmacokinetic parameters, as shown in Table 2.

Determination of Drug Concentration in Plasma

As described in Figure 6A, MTPOM reached a peak concentration in plasma of 2.05 ± 0.75 μg/mL at 1 h after the administration of the NS MTPOM-NS. Drug levels declined but remained elevated (in comparison to equivalent MTPOM-CS administration) after 2 and 6 h and were measurable up to 24 h, after which MTPOM was fully cleared from blood circulation. In contrast, the coarse formulation (MTPOM-CS) achieved a 4-fold lower peak plasma concentration of 0.49 ± 0.26 μg/mL at 2 h post administration. Thereafter, plasma levels abruptly declined, and were undetectable after 12 h. Notably, plasma MTPOM levels were consistently higher following nano-formulation administration, confirming the improved bioavailability conferred by the nanocrystal formulation. Consistently, absorption from the peritoneal cavity was significantly greater for MTPOM-NS, as depicted from the AUC $_{0-\infty}$ values (10.99 vs 2.15 μg/mL h for MTPOM-NS and MTPOM-CS,

Table 2 MTPOM PK Parameters After a Single I.p. Administration (5 mg/Kg) of MTPOM-NS and MTPOM-CMCS in Rats

	MTPOM-NS	MTPOM-CS
$T_{1/2}$ (h)	4.58 ± 1.53	1.5 ± 0.45
V_{ss} (L/kg)	3.04 ± 0.88	5.13 ± 1.63
CL (L/Kg/h)	0.53 ± 0.15	2.47 ± 0.77
T_{max} (h)	1.33 ± 0.43	1.67 ± 0.58
C_{max} (μg/mL)	2.07 ± 0.73	0.55 ± 0.17
AUC $_{0-\infty}$ (μg/mL · h)	10.99 ± 3.27	2.15 ± 0.73

Note: Data analysis performed via PK-Solver software.
Abbreviations: $T_{1/2}$, Elimination half-life; T_{max}, Time to reach maximum blood concentration; C_{max}, Maximum blood concentration; V_{ss}, Apparent volume of distribution at steady state; CL, Apparent clearance; $AUC_{0-\infty}$, the total area under the drug plasma concentration–time curve.

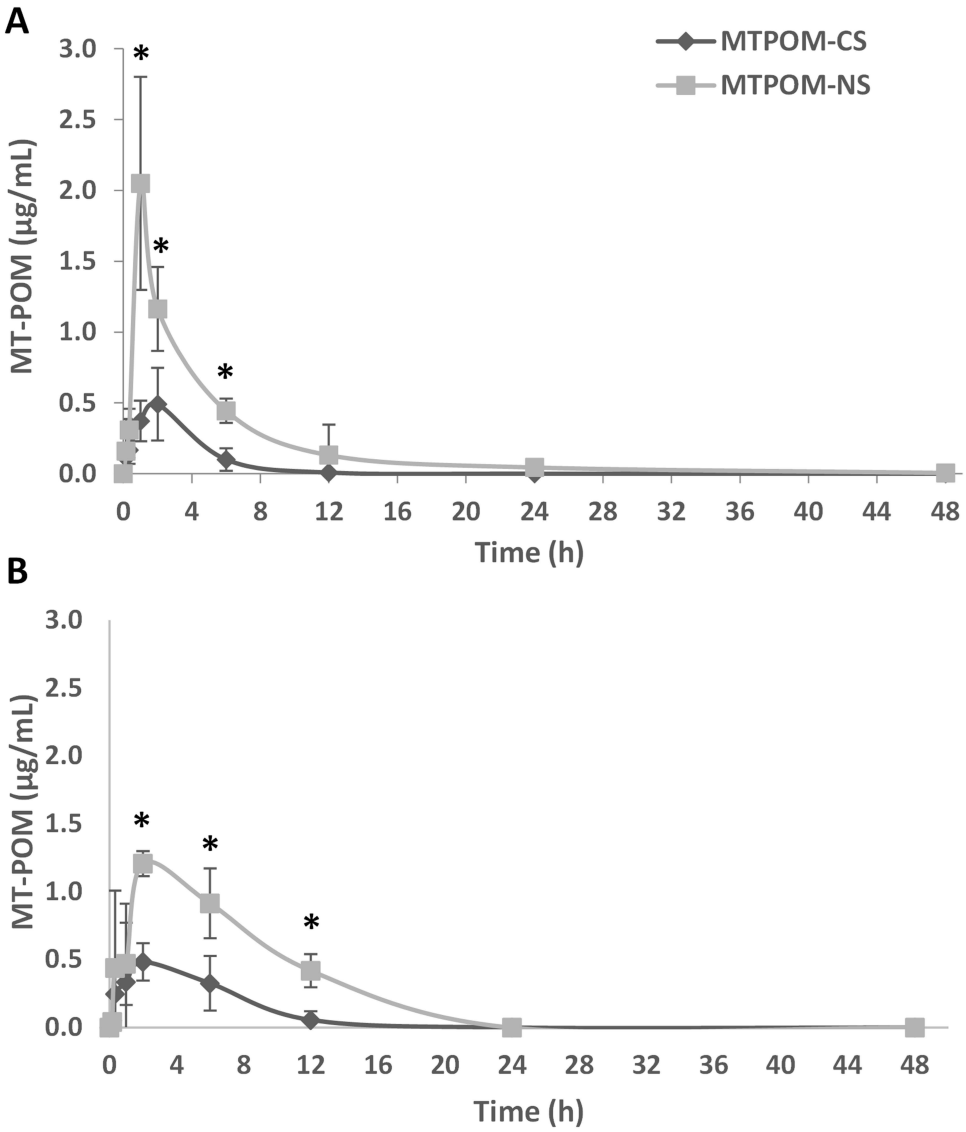

Figure 6 Plasma (**A**) and brain (**B**) MTPOM concentration at different time points (10, 20 min, 1, 2, 6, 12, 24 and 48 h) after a single dose (5 mg/kg) i.p. administration of MTPOM-NS or MTPOM-CS; (* $p < 0.05$ between plasma and brain values of the same timepoint).

respectively). Of additional interest, the elimination half-life ($T_{1/2}$) of MTPOM-NS was three-fold longer (4.58 h), as compared to equivalent administration of MTPOM-CS (1.50 h) (Table 2).

Determination of Drug Concentration in Brain

Given the potential of IMiDs as a treatment strategy for neurological disorders, one of the aims of the present study was to develop a drug formulation capable of enhancing brain bioavailability, as compared to coarse formulation. Hence, MTPOM brain concentrations were determined, as shown in Figure 6B.

Consistent with plasma data, the administration of MTPOM-NS led to higher brain concentration, in comparison to MTPOM-CS, at all time-points analyzed. Specifically, brain drug concentrations reached a peak at 2 h after intraperitoneal administration of either MTPOM-NS or MTPOM-CS, but were approximately three-fold greater with the nanoformulation across all time-points. Notably, MTPOM-NS remained detectable in brain tissue over 48 h, whereas the coarse suspension was more rapidly cleared by 12 h.

Interestingly, brain MTPOM levels achieved from the coarse formulation were, in large part, consistently comparable with concomitant plasma levels. In contrast, brain drug levels achieved by MTPOM-NS were double those in plasma 6 h after the

administration (Figure 7), suggesting potential drug accumulation within brain tissue and a slower brain clearance, as compared to the peripheral clearance, as similarly observed in our previous development of a pomalidomide NS.[42]

These findings confirm that nanosizing significantly improves both systemic bioavailability and brain penetration, which are critical factors for the efficacy of neurological therapeutics. Compared to our prior work with POM-NS[42] the current MTPOM-NS not only retains these pharmacokinetic benefits but also introduces a potentially safer pharmacological profile. This is largely due to MTPOM's selective engagement of CRBN, which, unlike POM, does not prompt the degradation of neosubstrates such as SALL4 and Aiolos, molecular mediators implicated in the teratogenic and oncogenic side effects of conventional IMiDs.[23] This selectivity addresses a critical safety concern that has limited the clinical utility of IMiDs for chronic neurological conditions.[45] By maintaining robust anti-inflammatory activity without triggering these adverse pathways, MTPOM promises to preserve therapeutic efficacy while minimizing risks associated with long-term administration. The prolonged brain tissue exposure and significant accumulation relative to plasma levels further support its potential as a CNS-targeted therapy.

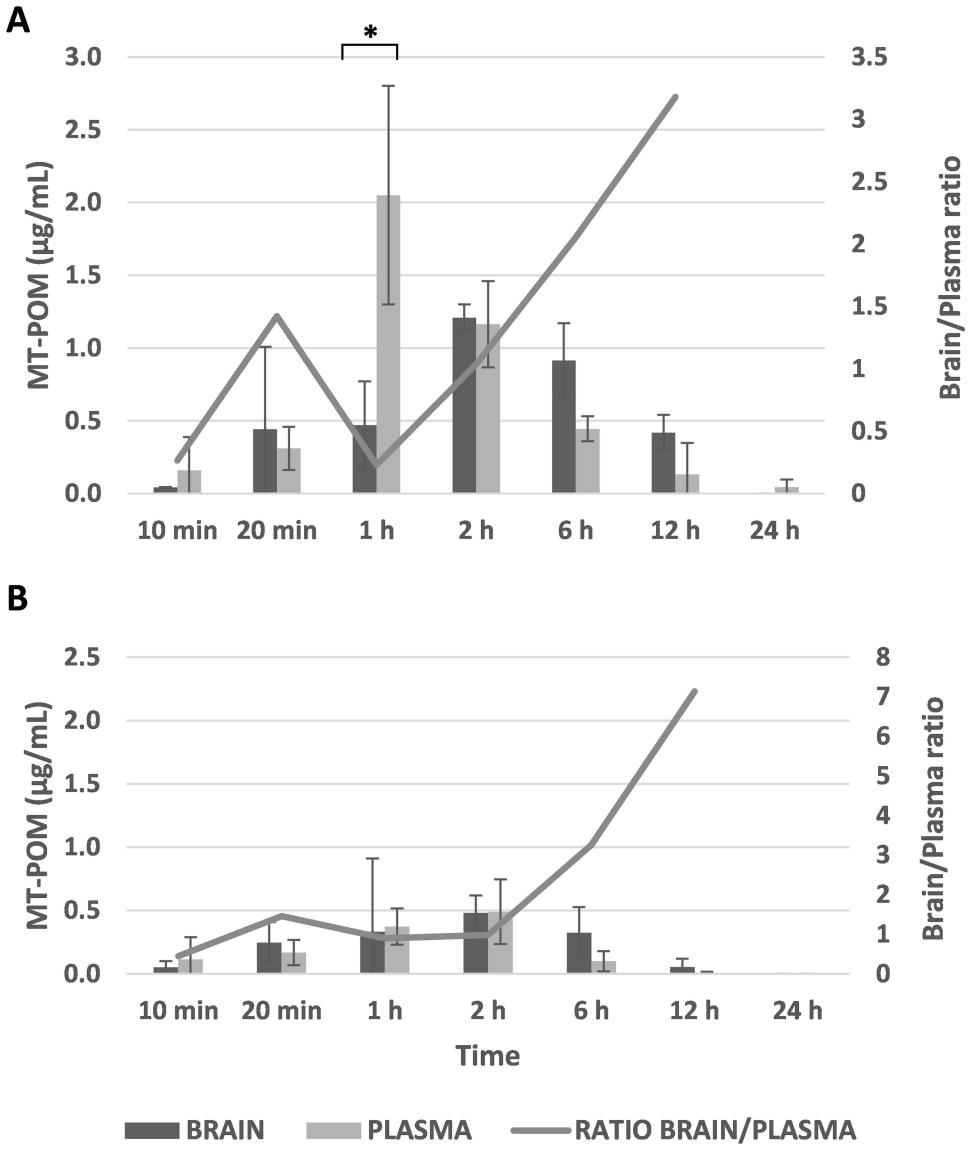

Figure 7 Plasma and brain MTPOM concentration after i.p. administration of MTPOM-NS (**A**) and MTPOM-CS (**B**) at different time points (10, 20 min, 1, 2, 6, 12, 24 and 48 h); (* $p < 0.05$).

Conclusions

The objective of this study was to overcome the poor aqueous solubility and limited bioavailability of the novel IMiD 3-monothiopomalidomide, by developing and characterizing a NS formulation (MTPOM-NS). We successfully produced a stable NS with uniform particle size, negative zeta potential, and preserved crystallinity. Compared to the raw drug and coarse suspension, MTPOM-NS demonstrated markedly improved solubility, rapid dissolution, and superior pharmacokinetic performance, achieving higher plasma concentrations, prolonged systemic exposure, and enhanced brain accumulation in rats following intraperitoneal administration in rats. The most significant finding is that MTPOM-NS provided sustained and elevated brain levels relative to plasma, highlighting its potential to accumulate within the CNS. These results, combined with the lower teratogenic risk of this compound, in comparison to clinically available IMiDs, positions MTPOM-NS as a promising drug candidate for the treatment neurological disorders with a neuroinflammatory component, as epitomized by PD, ischemic stroke and head injury.[11,12,63]

Data Sharing Statement

The data generated during the present study are available from the corresponding author upon reasonable request.

Acknowledgment

The authors acknowledge support from the University of Cagliari under Open Access funding call for the publication of this work.

Author Contributions

All authors made a significant contribution to the work reported, whether that is in the conception, study design, execution, acquisition of data, analysis and interpretation, or in all these areas; took part in drafting, revising or critically reviewing the article; gave final approval of the version to be published; have agreed on the journal to which the article has been submitted; and agree to be accountable for all aspects of the work.

Funding

This study was supported in part by the National Institute on Aging, Intramural Research Program (AG 000994).

Disclosure

Dong Seok Kim is employed by and has stock in Aevis Bio Inc.; also has a patent EP4484417A1 pending to Aevis Bio, Inc. Daejeon, Republic of Korea. All other authors declare that they have no known competing financial interests or personal relationships that could have appeared to influence the work reported in this paper.

References

1. Bradburn S, Murgatroyd C, Ray N. Neuroinflammation in mild cognitive impairment and Alzheimer's disease: a meta-analysis. *Ageing Res Rev*. 2019;50:1–8. doi:10.1016/j.arr.2019.01.002
2. Troncoso-Escudero P, Parra A, Nassif M, Vidal RL. Outside in: unraveling the role of neuroinflammation in the progression of Parkinson's disease. *Front Neurol*. 2018;9:1–15. doi:10.3389/fneur.2018.00860
3. Ransohoff RM. How neuroinflammation contributes to neurodegeneration. *Science*. 2016;353(6301):777–783. doi:10.1126/science.aag2590
4. Smith JA, Das A, Ray SK, Banik NL. Role of pro-inflammatory cytokines released from microglia in neurodegenerative diseases. *Brain Res Bull*. 2012;87(1):10–20. doi:10.1016/j.brainresbull.2011.10.004
5. Shabab T, Khanabdali R, Moghadamtousi SZ, Kadir HA, Mohan G. Neuroinflammation pathways: a general review. *Int J Neurosci*. 2017;127(7):624–633. doi:10.1080/00207454.2016.1212854
6. Martinez B, Peplow P. Neuroprotection by immunomodulatory agents in animal models of Parkinson's disease. *Neural Regen Res*. 2018;13(9):1493–1506. doi:10.4103/1673-5374.237108
7. Moore AH, Bigbee MJ, Boynton GE, et al. Non-steroidal anti-inflammatory drugs in Alzheimer's disease and Parkinson's disease: reconsidering the role of neuroinflammation. *Pharmaceuticals*. 2010;3(6):1812–1841. doi:10.3390/ph3061812
8. Grimmig B, Morganti J, Nash K, Bickford PC. Immunomodulators as therapeutic agents in mitigating the progression of Parkinson's disease. *Brain Sci*. 2016;6(4):41. doi:10.3390/brainsci6040041
9. Dong Y, Dekens DW, De Deyn PP, Naudé PJW, Eisel ULM. Targeting of tumor necrosis factor alpha receptors as a therapeutic strategy for neurodegenerative disorders. *Antibodies*. 2015;4(4):369–408. doi:10.3390/antib4040369

10. Mukherjee A, Biswas S, Roy I. Immunotherapy: an emerging treatment option for neurodegenerative diseases. *Drug Discov Today*. 2024;29 (5):103974. doi:10.1016/j.drudis.2024.103974
11. Jung YJ, Tweedie D, Scerba MT, et al. Repurposing Immunomodulatory Imide Drugs (IMiDs) in neuropsychiatric and neurodegenerative disorders. *Front Neurosci*. 2021;15:656921. doi:10.3389/FNINS.2021.656921
12. Jung YJ, Tweedie D, Scerba MT, Greig NH. Neuroinflammation as a factor of neurodegenerative disease: thalidomide analogs as treatments. *Front Cell Dev Biol*. 2019;7:1–24. doi:10.3389/fcell.2019.00313
13. Casu MA, Mocci I, Isola R, et al. Neuroprotection by the immunomodulatory drug pomalidomide in the drosophila LRRK2WD40 genetic model of Parkinson's disease. *Front Aging Neurosci*. 2020;12:31. doi:10.3389/fnagi.2020.00031
14. Majeed J, Sabbagh MN, Kang MH, et al. Cancer drugs with high repositioning potential for Alzheimer's disease. *Expert Opin Emerg Drugs*. 2023;28(4):311–332. doi:10.1080/14728214.2023.2296079
15. Streetly MJ, Gyertson K, Daniel Y, Zeldis JB, Kazmi M, Schey SA. Alternate day pomalidomide retains anti-myeloma effect with reduced adverse events and evidence of in vivo immunomodulation. *Br J Haematol*. 2008;141(1):41–51. doi:10.1111/J.1365-2141.2008.07013.X
16. Zhu YX, Kortuem KM, Stewart AK. Molecular mechanism of action of immune-modulatory drugs thalidomide, lenalidomide and pomalidomide in multiple myeloma. *Leuk Lymphoma*. 2013;54(4):683–687. doi:10.3109/10428194.2012.728597
17. Moreira AL, Sampaio EP, Zmuidzinas A, Frindt P, Smith KA, Kaplan G. Thalidomide exerts its inhibitory action on tumor necrosis factor alpha by enhancing mRNA degradation. *J Exp Med*. 1993;177(6):1675–1680. doi:10.1084/JEM.177.6.1675
18. Kopp KO, Greer ME, Glotfelty EJ, et al. A new generation of IMiDs as treatments for neuroinflammatory and neurodegenerative disorders. *Biomolecules*. 2023;13(5):1–34. doi:10.3390/biom13050747
19. Shi Q, Chen L. Cereblon: a protein crucial to the multiple functions of immunomodulatory drugs as well as cell metabolism and disease generation. *J Immunol Res*. 2017;2017:9130608. doi:10.1155/2017/9130608
20. Eichner R, Heider M, Fernández-Sáiz V, et al. Immunomodulatory drugs disrupt the cereblon-CD147-MCT1 axis to exert antitumor activity and teratogenicity. *Nat Med*. 2016;22(7):735–743. doi:10.1038/nm.4128
21. Lopez-Girona A, Mendy D, Ito T, et al. Cereblon is a direct protein target for immunomodulatory and antiproliferative activities of lenalidomide and pomalidomide. *Leukemia*. 2012;26(11):2326–2335. doi:10.1038/leu.2012.119
22. Chen KY, Hsueh SC, Parekh P, et al. 3-Monothiopomalidomide, a new immunomodulatory imide drug (IMiD), blunts inflammation and mitigates ischemic stroke in the rat. *GeroScience*. 2025;2025:1–21. doi:10.1007/s11357-025-01573-1
23. Hsueh SC, Parekh P, Batsaikhan B, et al. Targeting neuroinflammation: 3-monothiopomalidomide a new drug candidate to mitigate traumatic brain injury and neurodegeneration. *J Biomed Sci*. 2025;32(1):1–29. doi:10.1186/s12929-025-01150-w
24. Teo SK, Colburn WA, Tracewell WG, et al. Clinical pharmacokinetics of thalidomide. *Clin Pharmacokinet*. 2004;43(5):311–327. doi:10.2165/00003088-200443050-00004
25. Szabó ZI, Orbán G, Borbás E, et al. Inclusion complexation of the anticancer drug pomalidomide with cyclodextrins: fast dissolution and improved solubility. *Heliyon*. 2021;7(7):e07581. doi:10.1016/j.heliyon.2021.e07581
26. Pittiu A, Pannuzzo M, Casula L, et al. Production of liposomes by microfluidics: the impact of post-manufacturing dilution on drug encapsulation and lipid loss. *Int J Pharm*. 2024;664:124641. doi:10.1016/j.ijpharm.2024.124641
27. Rodriguez-Aller M, Guillarme D, Veuthey JL, Gurny R. Strategies for formulating and delivering poorly water-soluble drugs. *J Drug Deliv Sci Technol*. 2015;30:342–351. doi:10.1016/J.JDDST.2015.05.009
28. Aman A, Ali S, Mahalapbutr P, Krusong K, Wolschann P, Rungrotmongkol T. Enhancing solubility and stability of sorafenib through cyclodextrin-based inclusion complexation: in silico and in vitro studies. *RSC Adv*. 2023;13(39):27244–27254. doi:10.1039/d3ra03867j
29. Lombardo R, Ruponen M, Rautio J, et al. A technological comparison of freeze-dried poly-ε-caprolactone (PCL) and poly (lactic-co-glycolic acid) (PLGA) nanoparticles loaded with clozapine for nose-to-brain delivery. *J Drug Deliv Sci Technol*. 2024;93:105419. doi:10.1016/j.jddst.2024.105419
30. Casula L, Elena Giacomazzo G, Conti L, et al. Polyphosphoester-stabilized cubosomes encapsulating a Ru(II) complex for the photodynamic treatment of lung adenocarcinoma. *J Colloid Interface Sci*. 2024;670:234–245. doi:10.1016/j.jcis.2024.05.088
31. Mohammed PN, Hussen NH, Hasan AH, et al. A review on the role of nanoparticles for targeted brain drug delivery: synthesis, characterization, and applications. *EXCLI J*. 2025;24:34–59. doi:10.17179/EXCLI2024-7163
32. Hussen NH, Hasan AH, FaqiKhedr YM, Bogoyavlenskiy A, Bhat AR, Jamalis J. Carbon dot based carbon nanoparticles as potent antimicrobial, antiviral, and anticancer agents. *ACS Omega*. 2024;9(9):9849–9864. doi:10.1021/acsomega.3c05537
33. Ruggeri M, Sánchez-Espejo R, Casula L, et al. Bentonite- and palygorskite-based gels for topical drug delivery applications. *Pharmaceutics*. 2023;15(4):1253. doi:10.3390/pharmaceutics15041253
34. Mitrović JR, Divović-Matović B, Knutson DE, et al. Overcoming the low oral bioavailability of deuterated pyrazoloquinolinone ligand dk-i-60-3 by nanonization: a knowledge-based approach. *Pharmaceutics*. 2021;13(8):1188. doi:10.3390/PHARMACEUTICS13081188
35. Casula L, Sinico C, Valenti D, et al. Delivery of beclomethasone dipropionate nanosuspensions with an electronic cigarette. *Int J Pharm*. 2021;596:1–9. doi:10.1016/j.ijpharm.2021.120293
36. Müller RH, Jacobs C, Kayser O. Nanosuspensions as particulate drug formulations in therapy: rationale for development and what we can expect for the future. *Adv Drug Deliv Rev*. 2001;47:3–19 doi:10.1016/S0169-409X(00)00118-6.
37. Müller RH, Peters K. Nanosuspensions for the formulation of poorly soluble drugs. I. Preparation by a size-reduction technique. *Int J Pharm*. 1998;160(2):229–237. doi:10.1016/S0378-5173(97)00311-6
38. Van Eerdenbrugh B, Van den Mooter G, Augustijns P. Top-down production of drug nanocrystals: nanosuspension stabilization, miniaturization and transformation into solid products. *Int J Pharm*. 2008;364(1):64–75. doi:10.1016/j.ijpharm.2008.07.023
39. Casula L, Pireddu R, Cardia MC, et al. Nanosuspension-based dissolvable microneedle arrays to enhance diclofenac skin delivery. *Pharmaceutics*. 2023;15(9):2308. doi:10.3390/pharmaceutics15092308
40. Sinha B, Müller RH, Möschwitzer JP. Bottom-up approaches for preparing drug nanocrystals: formulations and factors affecting particle size. *Int J Pharm*. 2013;453(1):126–141. doi:10.1016/j.ijpharm.2013.01.019
41. Casula L, Schlich M, Cardia MC, et al. Design and bottom-up production of an aerosolizable cannabidiol nanosuspension. *Mol Pharm*. 2025;22 (1):498–508. doi:10.1021/acs.molpharmaceut.4c01095

42. Cardia MC, Palmas MF, Casula L, et al. Nanocrystals as an effective strategy to improve Pomalidomide bioavailability in rodent. *Int J Pharm*. 2022;625:122079. doi:10.1016/j.ijpharm.2022.122079
43. Palmas MF, Ena A, Burgaletto C, et al. Repurposing Pomalidomide as a Neuroprotective Drug: efficacy in an Alpha-Synuclein-Based Model of Parkinson's Disease. *Neurotherapeutics*. 2022;19(1):305–324. doi:10.1007/S13311-022-01182-2
44. Matyskiela ME, Couto S, Zheng X, et al. SALL4 mediates teratogenicity as a thalidomide-dependent cereblon substrate. *Nat Chem Biol*. 2018;14 (10):981–987. doi:10.1038/s41589-018-0129-x
45. Vargesson N. Thalidomide-induced teratogenesis: history and mechanisms. *Birth Defects Res Part C Embryo Today Rev*. 2015;105(2):140–156. doi:10.1002/BDRC.21096
46. Vargesson N. The teratogenic effects of thalidomide on limbs. *J Hand Surg Eur Vol*. 2019;44(1):88–95. doi:10.1177/1753193418805249
47. Mitrović JR, Divović-Matović B, Knutson DE, et al. Overcoming the low oral bioavailability of deuterated pyrazoloquinolinone ligand dk-i-60-3 by nanonization: a knowledge-based approach. *Pharmaceutics*. 2021;13(8):1–19. doi:10.3390/pharmaceutics13081188
48. Schlich M, Casula L, Musa A, et al. Needle-free jet injectors and nanosuspensions: exploring the potential of an unexpected pair. *Pharmaceutics*. 2022;14(5):1085. doi:10.3390/PHARMACEUTICS14051085
49. Sun J, Wang F, Sui Y, et al. Effect of particle size on solubility, dissolution rate, and oral bioavailability: evaluation using coenzyme Q 10 as naked nanocrystals. *Int J Nanomed*. 2012;7:5733–5744. doi:10.2147/IJN.S34365
50. Hao J, Gao Y, Zhao J, et al. Preparation and optimization of resveratrol nanosuspensions by antisolvent precipitation using box-behnken design. *AAPS Pharm Sci Tech*. 2014;16(1):118–128. doi:10.1208/S12249-014-0211-Y
51. Altalal A, Almomen A, Alkholief M, Binkhathlan Z, Alzoman NZ, Alshamsan A. Development and validation of a UPLC-MS/MS method for simultaneous detection of doxorubicin and sorafenib in plasma: application to pharmacokinetic studies in rats. *Saudi Pharm J*. 2023;31 (7):1317–1326. doi:10.1016/j.jsps.2023.05.025
52. Casula L, Craparo EF, Lai E, et al. Encapsulation of nanocrystals in mannitol-based inhalable microparticles via spray-drying: a promising strategy for lung delivery of curcumin. *Pharmaceuticals*. 2024;17(12):1708. doi:10.3390/ph17121708
53. FDA/CDER. Dissolution Testing of Immediate Release Solid Oral Dosage Forms. 1997. Available from: http://www.fda.gov/cder/guidance.htm. Accessed January 6, 2022.
54. EMA. CPMP/EWP/QWP/1401/98 Rev. 1. Guideline on the investigation of bioequivalence. 2010. Available from: http://www.ema.europa.eu. Accessed January 6, 2022.
55. Merisko-Liversidge E, Liversidge GG. Nanosizing for oral and parenteral drug delivery: a perspective on formulating poorly-water soluble compounds using wet media milling technology. *Adv Drug Deliv Rev*. 2011;63(6):427–440. doi:10.1016/j.addr.2010.12.007
56. Pramod K, Suneesh CV, Shanavas S, Ansari SH, Ali J. Unveiling the compatibility of eugenol with formulation excipients by systematic drug-excipient compatibility studies. *J Anal Sci Technol*. 2015;6(1):34. doi:10.1186/s40543-015-0073-2
57. Detroja C, Chavhan S, Sawant K. Enhanced antihypertensive activity of candesartan cilexetil nanosuspension: formulation, characterization and pharmacodynamic study. *Sci Pharm*. 2011;79(3):635–652. doi:10.3797/SCIPHARM.1103-17
58. Pawar VK, Singh Y, Meher JG, Gupta S, Chourasia MK. Engineered nanocrystal technology: in-vivo fate, targeting and applications in drug delivery. *J Control Release*. 2014;183(1):51–66. doi:10.1016/J.JCONREL.2014.03.030
59. Council of Europe. 5.17.1. Reccomendations on dissolution testing. In: *The European Pharmacopoeia*. 8th ed. 2013:727–729.
60. Liu P, Rong X, Laru J, et al. Nanosuspensions of poorly soluble drugs: preparation and development by wet milling. *Int J Pharm*. 2011;411 (1–2):215–222. doi:10.1016/J.IJPHARM.2011.03.050
61. Gao L, Zhang D, Chen M. Drug nanocrystals for the formulation of poorly soluble drugs and its application as a potential drug delivery system. *J Nanopart Res*. 2008;10(5):845–862. doi:10.1007/s11051-008-9357-4
62. Lukas G, Brindle SD, Greengard P. The route of absorption of intraperitoneally administered compounds. *J Pharmacol Exp Ther*. 1971;178 (3):562–564.
63. Palmas MF, Aminzadeh K, Runfola M, et al. A new therapeutic approach for Parkinson's disease: dual targeting of α-Synuclein aggregation and microglial function by the novel immunomodulator 3-Monothiopomalidomide. *Submitted*. 2025.